

12-2017

Vibronically Coherent Ultrafast Triplet-Pair Formation and Subsequent Thermally Activated Dissociation Control Efficient Endothermic Singlet Fission

Hannah L. Stern
University of Cambridge, UK


Alexandre Cheminal
University of Cambridge, UK

Shane R. Yost
University of California - Berkeley

Katharina Broch
University of Cambridge, UK

Sam L. Bayliss
University of Cambridge, UK

See next page for additional authors

Follow this and additional works at: https://uknowledge.uky.edu/chemistry_facpub
 [Click here to open a feedback form in a new tab to let us know how this document benefits you.](#)
Part of the [Chemistry Commons](#)

Repository Citation

Stern, Hannah L.; Cheminal, Alexandre; Yost, Shane R.; Broch, Katharina; Bayliss, Sam L.; Chen, Kai; Tabachnyk, Maxim; Thorley, Karl J.; Greenham, Neil; Hodgkiss, Justin; Anthony, John E.; Head-Gordon, Martin; Musser, Andrew J.; Rao, Akshay; and Friend, Richard H., "Vibronically Coherent Ultrafast Triplet-Pair Formation and Subsequent Thermally Activated Dissociation Control Efficient Endothermic Singlet Fission" (2017). *Chemistry Faculty Publications*. 154.
https://uknowledge.uky.edu/chemistry_facpub/154

Authors

Hannah L. Stern, Alexandre Cheminal, Shane R. Yost, Katharina Broch, Sam L. Bayliss, Kai Chen, Maxim Tabachnyk, Karl J. Thorley, Neil Greenham, Justin Hodgkiss, John E. Anthony, Martin Head-Gordon, Andrew J. Musser, Akshay Rao, and Richard H. Friend

Vibronically Coherent Ultrafast Triplet-Pair Formation and Subsequent Thermally Activated Dissociation Control Efficient Endothermic Singlet Fission**Notes/Citation Information**

Published in *Nature Chemistry*, v. 9, no. 12, p. 1205-1212.

© 2017 Macmillan Publishers Limited, part of Springer Nature. All rights reserved.

This is a post-peer-review, pre-copyedit version of an article published in *Nature Chemistry*. The definitive publisher-authenticated version Stern, H. L., Cheminal, A., Yost, S. R., Broch, K., Bayliss, S. L., Chen, K., ... Friend, R. H. (2017). Vibronically coherent ultrafast triplet-pair formation and subsequent thermally activated dissociation control efficient endothermic singlet fission. *Nature Chemistry*, 9, 1205-1212. <https://doi.org/10.1038/nchem.2856> is available online at: <https://doi.org/10.1038/nchem.2856>.

Digital Object Identifier (DOI)

<https://doi.org/10.1038/nchem.2856>

1

2 **Vibronically coherent ultrafast triplet-pair formation and**
3 **subsequent thermally activated dissociation control efficient**
4 **endothermic singlet fission.**

5

6 Hannah L. Stern*¹, Alexandre Cheminal¹, Shane R. Yost^{2,3}, Katharina Broch¹, Sam L.
7 Bayliss¹, Kai Chen^{4,5}, Maxim Tabachnyk¹, Karl Thorley⁶, Neil Greenham¹, Justin
8 Hodgkiss^{4,5}, John Anthony⁶, Martin Head-Gordon^{2,3}, Andrew J. Musser¹, Akshay Rao¹
9 and Richard H. Friend¹.

10

11 ¹ Cavendish Laboratory, University of Cambridge, UK.

12 ² Kenneth S. Pitzer Center for Theoretical Chemistry, Department of Chemistry, University of
13 California, Berkeley, USA.

14 ³ Chemical Science Division, Lawrence Berkeley National Laboratory, Berkeley, USA.

15 ⁴ MacDiarmid Institute for Advanced Materials and Nanotechnology, New Zealand.

16 ⁵ School of Chemical and Physical Sciences, Victoria University of Wellington, New Zealand.

17 ⁶ University of Kentucky, Lexington, USA.

18

19

20

21

22

23

24

25 **Abstract**

26 Singlet exciton fission (SF), the conversion of one spin-singlet exciton (S_1) into two
27 spin-triplet excitons (T_1), could provide a means to overcome the Shockley-Queisser
28 limit in photovoltaics. SF as measured by the decay of S_1 has been shown to occur
29 efficiently and independently of temperature even when the energy of S_1 is as much
30 as 200 meV less than $2T_1$. Here, we study films of TIPS-tetracene using transient
31 optical spectroscopy and show that the triplet pair state (TT), which has been
32 proposed to mediate singlet fission, forms on ultrafast timescales (in 300 fs) and that
33 its formation is mediated by the strong coupling of electronic and vibrational degrees
34 of freedom. This is followed by a slower loss of singlet character as the excitation
35 evolves to become only TT. We observe the TT to be thermally dissociated on 10-
36 100 ns timescales to form free triplets. This provides a model for ‘temperature
37 independent’, efficient TT formation and thermally activated TT separation.

38

39 Singlet exciton fission (SF) is a quantum mechanical phenomenon unique to organic
40 chromophores that could provide a route to breaking the Shockley-Queisser limit on
41 the efficiency of single junction photovoltaics (PVs)^{1,2,3}. In this process, a
42 photogenerated spin-0 singlet exciton (S_1) is converted to two spin-1 triplet excitons
43 (T_1). It has been proposed that this conversion is mediated by a triplet pair
44 intermediate state (TT), which forms an overall spin-0 state⁴. This means that SF does
45 not require a spin flip and can proceed on <100 fs timescales when SF is exothermic,
46 i.e $E(S_1) > 2E(T_1)$, allowing for near unity efficiency (200% triplet yield) in materials
47 such as pentacene⁵.

48

49 But intriguingly, SF also proceeds very efficiently in endothermic systems, where
50 $E(S_1) < 2E(T_1)$, overcoming energy barriers ($E_b = 2E(T_1) - E(S_1)$) of up to 200 meV⁶.
51 Such systems are of particular technological importance, as most of the materials with
52 $E(T_1)$ comparable to the bandgap of silicon (1.1eV) fall into this category, including
53 perylenediimides⁷ and acenes such as tetracene ($E_b \cong 180$ meV), which is the most
54 well studied endothermic SF system^{6,8,9}. Extensive work by Bardeen and others has
55 unambiguously shown that free triplets are produced in a high yield in polycrystalline
56 tetracene, yet S_1 decays independently of temperature on a 70-90 ps timescale^{6,10,11,12}.
57 The rate of decay is three orders of magnitude slower than in pentacene, despite
58 similar electronic couplings between the relevant electronic states¹³. So, what controls
59 the decay rate of S_1 and how can this state efficiently overcome an endothermic
60 barrier to generate free triplets?

61

62 To investigate the mechanism of endothermic SF we study solid-state TIPS-
63 tetracene¹⁴, which has the same molecular core as tetracene but is made solution

64 processable via the addition of triisopropylsilyl (TIPS) ethynyl side groups, see Figure
65 1b. As we discuss below, TIPS-tetracene possesses sharp signatures for S_1 and T_1
66 states. We use ultrafast spectroscopy to show that the photoexcited population
67 acquires TT character on sub-300 fs timescales and evolves to lose S_1 character on a
68 morphology-dependent 6-20 ps timescale. The TT state is long-lived and thermally
69 dissociates into separated T_1 on 10 ns timescales in disordered films at room
70 temperature, but surprisingly, remains bound for tens of μ s in polycrystalline films
71 due to a low triplet-hopping rate.

72

73 **Results and Discussion**

74 **Ultrafast TT formation**

75 Figure 1a shows the energetics of TIPS-tetracene, where the energies of S_1 (2.3 eV)
76 (from UV-Vis absorption) and T_1 (1.20-1.30 eV) (from phosphorescence)¹⁵, indicate
77 that fission is similarly endothermic to tetracene. In this study we investigate two
78 film types, 'disordered' and 'polycrystalline' that differ in morphology (see SI for
79 structural characterization). The UV-Vis and photoluminescence spectra of TIPS-
80 tetracene dilute solution, disordered and polycrystalline films are shown in Figure 1c.
81 The TIPS-tetracene chemical and crystal structure is shown in Figure 1b.

82

83 To investigate the dynamics of SF we use ultrafast broadband transient absorption
84 (TA) spectroscopy with 16 fs time resolution. Figures 2a and b show the room-
85 temperature TA spectra from 50 fs to 2 ps of the two film types, optically excited
86 close to the absorption edge. The spectral shapes observed in both films are consistent
87 with the S_1 and TT species previously identified in concentrated solutions of TIPS-
88 tetracene¹⁵. The initial positive signal at 570 nm (Figures 2a and b) is consistent with

89 photoluminescence maximum of the 0-1 band of the S_1 emission and is assigned to S_1
90 stimulated emission (SE), as seen for dilute solution (Figure 2c). The broad negative
91 signal from 600-1300 nm corresponds mainly to S_1 photo-induced absorption (PIA)
92 and is similar to the solution.

93

94 At longer time delays we observe a sharply peaked absorption spectrum (90ps time
95 slice in fig 2a and b) that is assigned to the TT state. This assignment is based on the
96 results from the previous solution study revealing that the T_1 absorption in TIPS-
97 tetracene shows sharp peaks across the visible and NIR(, regularly spaced by a
98 vibrational frequency of $\sim 1300\text{ cm}^{-1}$). The TT state was shown to display the same
99 sharp T_1 absorption peaks, but shifted by up to 5 meV¹⁵. The assignments of S_1 and
100 TT to the spectral species are based on the similarity of the spectral features we
101 observe to those of individual S_1 and T_1 excitons in solution, but does not preclude
102 mixing of CT states, which our spectroscopic measurements can not give information
103 on, into these states¹³.

104

105 In Figure 2c we present the TT absorption spectrum at 100 ps obtained from a TA
106 measurement of the polycrystalline film. Notably, the sharp TT absorption bands at
107 670, 850 nm and 960 nm enable us to track the conversion of S_1 to TT.

108

109 Figure 2d and 2e show the loss of S_1 SE and growth of the TT absorption for the two
110 film types over the first 2 ps. To single out the TT growth we use kinetics at 860 nm
111 and 835 nm, at the maximum and to the side of the sharp TT absorption band (see TT
112 absorption in Figure 2c) and normalise to the peak initial signal when only S_1 is
113 present. The difference between the two kinetics provides a background-free kinetic

114 and captures TT population evolution. Both films show a rise time of 250 fs for the
115 TT absorption that is matched by the rate of loss of SE intensity at 570-580 nm. We
116 confirm this time for the ultrafast interconversion of S_1 and TT using a spectral
117 deconvolution method that takes into account all spectral changes across the visible-
118 NIR region (see Supplementary Information section 5). At longer times, there is a
119 further ~10 ps rise in the TT state, matching the decay of S_1 .

120

121 **Vibrationally coherent TT formation**

122 The ultrafast pump pulse impulsively excites the system as has been discussed
123 previously¹⁶. This vibrational coherence results in strong oscillations in the TA
124 spectra and kinetics, as seen in Figure 2d-e. We globally fit the population decay for
125 the TA measurements and Fourier transform the residuals that contain the modulation
126 on top of the electronic response (Supplementary Fig. 14). In Figure 3a we compare
127 these Fourier spectra obtained from integration across the whole optical spectrum of
128 both film types (560 –1300 nm) with dilute solution (grey trace) and the ground state
129 resonance Raman spectrum (black trace).

130

131 The presence of additional modes in the films in comparison with solution results
132 from additional excited states present in the films that are absent in dilute solutions.
133 To explore this, we compare the 315 cm^{-1} mode which is associated with the S_1 state
134 as seen in the dilute solution, with the 760 cm^{-1} mode that is only present in the films.
135 We plot the strength of these modes as a function of wavelength in Figure 3b, for
136 polycrystalline films that afford the best signal to noise. These plots show which parts
137 of the spectrum the modes are associated with and hence which excited states they are
138 coupled with. As can be seen in Figure 3b, the distribution of the 315 cm^{-1} mode

139 reveals nodes at the positions of maximum absorption intensity of the polycrystalline
140 film at early time delays when the system is dominated by S_1 , as expected in the case
141 where the 315 cm^{-1} mode is related to the lateral shifting of the S_1 absorption
142 spectrum (Supplementary Fig. 17)¹⁷. The 315 cm^{-1} mode also shows intensity at lower
143 energies ($\sim 1300\text{ nm}$) where there is a strong S_1 PIA. In contrast, the intensity of the
144 760 cm^{-1} mode is strongest in the 600 nm - 900 nm region, with a node at 860 nm ,
145 where there is a sharp TT PIA, and is very weak at wavelengths $> 1000\text{ nm}$, where the
146 TT state does not absorb strongly. This mode is absent in the vibrational spectra of
147 dilute solutions where SF does not occur and no TT state is formed.

148

149 In Figure 3c we present sliding-window Fourier transform plots of the 315 cm^{-1} and
150 760 cm^{-1} modes. This analysis uses a 1 ps -wide sliding window, represented on the x
151 axis by the earliest time point in the window. The 315 cm^{-1} mode is plotted for 570
152 nm and the 760 cm^{-1} mode is plotted for 850 nm , the regions associated with SE and
153 strong TT absorption in the polycrystalline films respectively. We find the 315 cm^{-1}
154 mode shows a decrease over time, as expected for a mode where vibrational
155 coherence is generated upon photoexcitation and subsequently damped, either by
156 movement away from the S_1 PES or by scattering on the phonon bath. Scattering is
157 unlikely, as damping times for this phenomenon are expected to be on the picosecond
158 timescale. In contrast, the 760 cm^{-1} mode shows an initial increase, as the window
159 slides from 0 - 1 ps to 0.4 - 1.4 ps . The time period of the 760 cm^{-1} mode, 43 fs , is much
160 shorter than the TT rise time (250 fs), which means that vibrational coherence cannot
161 be created impulsively via the SF process populating TT. Rather, the 760 cm^{-1} mode
162 is likely to be a product mode of the reaction, formed as the nuclear wavepacket
163 moves from the S_1 to the TT PES. Hence, the increase in strength seen in Figure 3c as

164 the underlying TT state grows in (Figure 2e) indicates the formation of the TT state
165 occurs via a vibrationally coherent process. This is similar to vibrationally coherent
166 SF observed in exothermic SF systems, which has been explored both
167 theoretically^{18,19}, and experimentally^{20,21,22}, and also vibrationally coherent ultrafast
168 internal conversion in polyenes²³ and energy transfer in biological light harvesting
169 systems²⁴.

170

171 This coupling also modulates the energy levels of the states involved in the SF
172 process, which is likely to help drive TT formation, as has been previously suggested
173 in a computational study of tetracene derivatives²⁵. The shifting of the PIA features in
174 the ultrafast TA spectra reveal that the transition energies over all excited states
175 present are modulated by more than 100 meV (Supplementary Fig. 14), indicating
176 that energies calculated with the ground state geometries do not provide a good guide
177 to understanding what happens on the excited state PES.

178

179 Our observations show that vibrational modes are involved in the rapid formation of
180 TT in TIPS-tetracene. This is different from a model based on strong-electronic
181 coupling between S_1 and TT, which has previously been invoked to explain the
182 dynamics of tetracene by Zhu et al.²⁶. Instead of the direct formation of a
183 superposition of S_1 and TT upon photoexcitation, our data suggest that following
184 photoexcitation vibrational modes drive the wavepacket from the initially populated
185 Frank-Condon region, modulating both the energies and couplings between S_1 and TT
186 and leading to the evolution of the state from one dominated by S_1 character to one
187 dominated by TT character. While such a process is known for exothermic
188 fission, where $2xT_1$ is lower in energy than S_1 , these results show how even

189 in endothermic systems the TT state can be accessed on ultrafast timescales, enabling
190 endothermic fission to be equally efficient at generating triplet excitons.

191

192 As seen in Figure 2d and 2e, following the early time ultrafast conversion of S_1 to TT,
193 there is delayed rise in TT with a concomitant decay of S_1 . This slower S_1 decay is
194 reminiscent of the S_1 decay observed in tetracene^{6,10} – it decays independently of
195 temperature over tens of picoseconds (see Supplementary Fig. 23-24) and shows a
196 morphology-dependent lifetime (6-10 ps for disordered and 15-19 ps for
197 polycrystalline), matching the delayed rise of TT. Correspondingly, a 11 ± 1 ps and
198 12 ± 1 ps photoluminescence lifetime was measured for the disordered and
199 polycrystalline film types respectively (Supplementary Fig. 10). The variation in
200 lifetime for the S_1 decay we observe between the TA and PL, and within the TA
201 measurements, we consider to arise due to the inhomogeneity across the
202 polycrystalline film. Importantly, in the absence of higher time resolution and sharp
203 TT spectral signatures this S_1 decay time would appear to be the SF rate for TIPS-
204 tetracene. However, as we have shown, this S_1 decay rate gives a misleadingly slow
205 indication of the rate of initial TT formation.

206

207 We consider that the ultrafast formation of TT represents SF that occurs at
208 photoexcited sites in the film where intermolecular arrangement is optimal for SF.
209 The picosecond morphology-dependent loss of S_1 and rise of TT may to be related to
210 the time needed for the excitation to diffuse to optimal fission geometries, as has been
211 suggested in tetracene^{10,27}. Multiple timescales for TT formation have also been
212 observed in hexacene²², where fission is exothermic, and most recently in rubrene²⁸,
213 where in both cases the two timescales of TT formation have been attributed to both

214 coherent and incoherent fission processes. In the later study, it was suggested that
215 coherent TT formation was related to excitation of low-frequency symmetry breaking
216 intermolecular modes, which was followed by a separate incoherent TT formation
217 pathway²⁸. However, in TIPS-tetracene we cannot rule out an alternate explanation
218 for the slow loss of S_1 that is also consistent with our data, whereby vibronic coupling
219 sets up an equilibrium between S_1 and TT and the 6-19 ps timescale is related to the
220 time needed to fully shift the S_1 -TT equilibrium to only TT. Such a process could be
221 mediated by slow damping of certain low-energy phonon modes that are associated
222 with the photoexcited state and not present within the crystal in the ground state, and
223 thus cannot be easily damped. This could allow for a vibronic equilibrium between S_1
224 and TT to be setup, which would last as long as the modes are undamped. Damping of
225 vibrational modes over 10s of ps has been previously observed at low temperature in
226 pentacene crystals in naphthalene²⁹. This hypothesis would be supported by our
227 observation that the broad PIA (600 nm-1300 nm) in the two films does not show the
228 prompt loss of oscillator strength as seen the SE feature, but shows many sharp
229 features associated with TT from sub-200fs timescales and decays over the
230 picosecond timescale (Figure 2a and b). We predict that the ultrafast TT formation is
231 associated with rapid movement away from the Franck Condon region resulting in
232 loss of SE and that the broad PIA features are due to absorption of the resulting S_1 -TT
233 state to higher-lying excited states.

234

235 **Thermally activated TT dissociation**

236 The fast formation dynamics indicate that the initial TT yield could be very high, as it
237 outcompetes radiative and non-radiative decay channels. However, it is the yield of T_1
238 + T_1 at longer timescales that is more relevant for photovoltaic device applications.

239 Figure 4e tracks the evolution of both films at 850 nm from 10 ps to 2 ms. In the
240 disordered film, the raw TA kinetic shows the presence of two decay regimes that we
241 can spectrally resolve, using a spectral deconvolution code based on a genetic
242 algorithm³⁰, into the decay of bound TT state ($\tau= 10$ ns (295 K)) and the decay of
243 separated T_1 ($\tau= 10$ μ s (295 K)) (Figure 4b). The near-IR spectra of the concentrated
244 solution, disordered film and polycrystalline film are shown in Figure 4(a,c,e). For the
245 concentrated solution and disordered film we observe a shifting of the TT absorption
246 peaks and loss of absorption between the two peaks over 1 ns - 1 μ s, to give the
247 absorption confirmed via sensitisation to be T_1 at microsecond delays¹⁵. A shift in the
248 TT absorption peaks have also been observed in pentacene derivatives and associated
249 with the changing excitonic interactions of the bound state as it separates³¹. However,
250 in the disordered film of TIPS-tetracene the TT dissociation rate and the yield of $T_1 +$
251 T_1 are both temperature-dependent (Figure 4b). As the temperature is lowered we
252 observe slower TT decay and relatively weaker $T_1 + T_1$ absorption, consistent with a
253 thermally activated TT separation. At the lowest temperatures measured (10 K), we
254 resolve only the TT state. We note that the room temperature TT lifetime measured
255 here is comparable to the TT lifetime in concentrated solution (8.7 ns)¹⁵, indicating
256 that a similar barrier is overcome in both systems. We make two estimates for the
257 yield of the reaction TT to $T_1 + T_1$. From the quenching of the TT PL at room
258 temperature (see below), we obtain a value of 180 ± 10 %, and from the evolution of
259 the TA, using T_1 cross-sections obtained from sensitization measurements a value of
260 130 ± 20 % (see Supplementary Information section 7).

261

262 The TT absorption, including the weaker TT feature at 900 nm, decays more slowly
263 and is present over the full decay in the polycrystalline film, Figure 4e. Furthermore,

264 the spectrum cannot be de-convoluted into multiple species. The decay of the
265 spectrum does not show an evident temperature dependence, nor is its decay
266 accelerated under increased fluence (from 80-400 μJcm^{-1}). Taken together, these
267 observations suggest that in polycrystalline films the TT state does not dissociate to
268 $T_1 + T_1$ even at room temperature.

269

270 To understand why the crystalline morphology gives rise to a long-lived TT state, we
271 calculate the triplet-hopping rates in two distinct intermolecular situations that
272 represent the extreme case for structure difference between the polycrystalline and
273 disordered films - two molecules from the crystal structure and two pi-pi stacked
274 dimers, respectively (see Supplementary Information section 2 for details). We find
275 that the two intermolecular geometries present very different hopping integrals: 15
276 and 0.2 meV for the pi-stacked dimer and the crystal structure respectively. Using a
277 reorganization energy of 0.33 eV and the Marcus model³² these hopping integrals
278 correspond to a T_1 hopping time of 2.5 ps and 52 ns, respectively. As we cannot know
279 how large or dense the pi-stacked domains are in the disordered film, this value
280 represents an upper limit. Importantly, these calculations highlight the unusually poor
281 triplet-triplet coupling in the TIPS-tetracene crystal structure and suggest that in
282 polycrystalline films, triplet hopping is very slow and significantly slow the
283 dissociation of the bound TT state.

284

285 **Photoluminescence from the TT state**

286 Photoluminescence measurements also reveal information on the energetics and
287 evolution of the TT state. The photoluminescence quantum efficiency in both film
288 types is moderately low: 3% and 1% for the disordered and polycrystalline films

289 respectively, at room temperature. However, as we report below, the PL yield for the
290 disordered film increases rapidly with reducing temperature, by a factor of 20 at 10 K,
291 implying a PL yield of around 60%. Fig. 5c and 5f show the temperature-dependent
292 steady-state PL of the two films. The disordered film shows a broad PL centered at
293 ~650 nm, with two vibronic peaks clearly visible at low temperature. The
294 polycrystalline film shows three different peaks, and the overall temperature-
295 dependent behavior is similar to tetracene^{5,6}, with the second peak at 580 nm
296 dominating at higher temperatures and the high-energy feature at 540 nm, associated
297 with the 0-0 transition of S₁ dominating at low temperature.

298

299 The time-resolved PL at 10 K reveals that in both film types there are two emissive
300 species, a prompt high-energy component, and a red-shifted emissive state (time
301 slices at 0.5 ns and 50 ns in Figure 5a and 5d). The high-energy state has the same
302 spectrum as the dilute solution and decays with a temperature-independent lifetime
303 (Figure 5b and 5e); we assign this to emission from S₁ in both disordered and
304 polycrystalline films. For the crystalline film, the S₁ feature has a delayed component,
305 similar to the well-studied delayed PL in tetracene^{6,33}. For the disordered film, no
306 delayed component of S₁ is detected, indicating that any regeneration of the S₁ from
307 TT is too weak to detect.

308

309 In both films the red-shifted emission region shows a thermal-dependence. From the
310 kinetic traces at 650 nm of the disordered film we obtain an activation energy, out of
311 the red-shifted emissive state, of ~90 meV (Supplementary Fig. 8). This temperature-
312 dependent emission tracks the temperature dependence for the TT state we observe in
313 TA (Figure 4b). We note that the high PL yield from the red-shifted emission in the

314 disordered film at 10 K allows direct comparison of the PL decay with the time
315 evolution of the TA spectra. As shown in Figure 4d the PL decay occurs on a 50 ns
316 timescale and matches the TT state decay measured via TA, as seen in solution
317 (Figure 4b). We thus consider that the red-shifted emission in the disordered film also
318 derives from the TT state. We note that 50 ns lifetime with 60% PL yield at 10K
319 suggests a radiative lifetime for the TT state in the disordered film of 80 ns. From the
320 PL yield in the disordered film, we can estimate the yield of the reaction TT to $T_1 +$
321 T_1 to be ~180%.

322

323 For both films, the red-shifted species shows pronounced vibronic structure, as
324 observed in a recent study of singlet fission in heteroacenes undergoing fission³⁴.
325 These are sharper in the polycrystalline material and broadened in the disordered,
326 where the emission has the same spectrum as the TT emission in concentrated
327 solution (Fig. S14). We therefore predict that the weak, red-shifted emission in the
328 polycrystalline film is also due to the TT state and that the transition dipole moment
329 of the TT state in the polycrystalline film is significantly reduced compared to the
330 disordered material. This is likely to be due to the ability of the molecules in the
331 disordered film to rearrange into an excimer-like TT state geometry that can more
332 easily radiatively couple to the ground state.

333

334 The activation energy we extract for TT dissociation from the PL measurements (50-
335 90 meV), is comparable to the activation energies measured for tetracene using PL
336 and TA (40-70 meV)^{35,36}. Taking into account the entropic gain following the
337 dissociation of TT to free triplets, which has been discussed by others^{26,36}, we expect

338 the activation energy to be one half of the value of E_b which we estimate to be 200
339 meV.

340

341 **Conclusions**

342 In summary, we have tracked the photophysical behavior of TIPS-Tetracene over ten
343 orders of magnitude (Figure 6) and our results show that ultrafast, activation-less
344 formation of stabilized, long-lived TT states, that quench radiative losses via S_1 and
345 protect the excitation from competing decay channels, is key to efficient endothermic
346 formation of $T_1 + T_1$. These states can be formed on sub 300 fs timescales, the
347 ultrafast conversion mediated by vibronic coupling. These results unify the
348 observation in tetracene of the simultaneous ultrafast rise of S_1 and multiexciton
349 features by Zhu et al. by photoelectron spectroscopy²⁶ with the slower S_1 dynamics
350 observed in optical measurements^{6,10,12}. At later times, the long-lived TT states can be
351 thermally dissociated to free T_1 , if the crystal morphology supports efficient triplet
352 hopping. If not, TT can remain bound on μ s timescales without being dissociated to
353 free T_1 . These results pave the way for further studies of how the optimisation of the
354 chemical structure of endothermic fission materials can alter vibronic coupling and
355 the ultrafast fission process.

356

357 **Methods**

358 **Sample preparation.** TIPS-tetracene was synthesized according to the procedure in
359 reference³⁷. For all of the optical measurements TIPS-tetracene was either spin coated
360 or drop cast onto 13 mm diameter fused silica substrates in an oxygen free
361 environment. Samples were measured under vacuum or, for low temperature
362 measurements, in a helium dynamic flow cryostat.
363

364 **Spectroscopic measurements.** UV-Vis absorption spectra were measured on a Cary
365 400 UV-Visible Spectrometer over the photon energy range 1.55 eV-3.54 eV. Steady-

366 state photoluminescence spectra were collected using a pulsed laser at 2.64 eV
367 (PicoQuant LDH400 40 MHz) and collected on a 500 mm focal length spectrograph
368 (Princeton Instruments, SpectraPro2500i) with a cooled CCD camera. Time-resolved
369 photoluminescence decay was measured using time-correlated single photon counting
370 (TCSPC), an intensified CCD camera (ICCD) and a transient grating set-up (TGPL).
371 For all measurements the sample was measured in either a side-on or backward
372 reflection geometry, to mitigate self-absorption. The TCSPC set-up uses the same
373 excitation source and camera as the steady-state PL and has a temporal resolution of
374 300 ps. Transient grating measurements were measured by a home-built transient-
375 grating photoluminescence spectroscopy, setup described elsewhere³⁸. The
376 photoluminescence quantum efficiencies of the films were measured using an
377 integrating sphere and a 2.33 eV excitation source. Picosecond and nanosecond
378 transient absorption spectra were recorded on a setup that has been previously
379 reported³⁹. The ultra-fast (20 fs) transient absorption experiments were performed
380 using a Nd :YAG based amplified system (PHAROS, Light Conversion) providing
381 14.5W at 1025 nm and 38 kHz repetition rate. See the supplementary information
382 section 1b for more details on the transient absorption setups.

383
384 **Structural measurements.** Grazing incidence wide angle X-ray scattering
385 measurements were performed at beamline I07, Diamond Light Source, UK, using a
386 Pilatus 1M detector and beam energy of 12.5 keV. X-ray diffraction measurements
387 were performed using a Bruker D8 setup and a wavelength of 1.5406 angstrom
388

389 **Data availability.** The data sets generated during and/or analysed during the current
390 study are available in the University of Cambridge data repository at
391 <https://doi.org/xxxx>.

392

393 **References**

- 394 (1) Smith, M. B.; Michl, J. Singlet fission. *Chem. Rev.* **110**, 6891–6936 (2010)
395 (2) Pope, M.; Swenberg, C. *Electronic Processes in Organic Crystals and*
396 *Polymers*; Oxford University Press (1999)
397 (3) Hanna, M. C.; Nozik, a. J. Solar conversion efficiency of photovoltaic and
398 photoelectrolysis cells with carrier multiplication absorbers, *J. App. Phys.* **100**,
399 074510 (2006)
400 (4) Merrifield RE. Magnetic Effects on Triplet Exciton Interactions. *Pure App.*
401 *Chem.* **27**, 481–498 (1971)
402 (5) Wilson, M.W.B.; Rao A.; Clark. J.; Kumar R. S. S.; Brida D.; Cerullo G.;
403 Friend R.H. Ultrafast dynamics of exciton fission in polycrystalline pentacene. *JACS*
404 **133**, 11830-11833 (2011)
405 (6) Burdett, J. J.; Gosztola, D.; Bardeen, C. J. The dependence of singlet exciton
406 relaxation on excitation density and temperature in polycrystalline tetracene thin
407 films: kinetic evidence for a dark intermediate state and implications for singlet
408 fission. *J. Chem. Phys.* **135**, 214508 (2011)
409 (7) Eaton, S.W.; Shoer, L. E.; Karlen, S. D.; Dyar, S. M.; Margulies, E. A.;
410 Veldkamp, B. S.; Ramanan, C.; Hartzler, D. A.; Savikhin, S.; Marks, T. J.;
411 Wasielewski, M. R.; Singlet exciton fission in polycrystalline thin films of a slip-
412 stacked perylenediimide. *JACS* **135**, 14701-14712 (2013)
413 (8) Swenberg, C. E.; Stacy, W. T. Bimolecular radiationless transitions in
414 crystalline tetracene. *Chem. Phys. Lett.* **2**, 327 (1968)

- 415 (9) Merrifield, R. E. Theory of magnetic field effects on the mutual annihilation of
416 triplet excitons. *J. Chem. Phys.* **48**, 4318 (1968)
- 417 (10) Piland, G. B.; Bardeen, C. J. How morphology Affects Singlet Fission in
418 Crystalline Tetracene. *J. Phys. Chem. Lett.* **6**, 1841–1846 (2015)
- 419 (11) Burdett, J.J.; Muller, A.M.; Gosztola, D.; Bardeen, C.J.; Excited state
420 dynamics in solid and monomeric tetracene: The roles of superradiance and exciton
421 fission. *J. Chem. Phys.* **133**, 144506 (2010)
- 422 (12) Wilson, M. W. B.; Rao, A.; Johnson, K.; Gelinas, S.; di Pietro, R.; Clark, J.;
423 Friend, R. H. [SEP] Temperature-independent singlet exciton fission in tetracene. *JACS*
424 **135**, 16680–8 (2013)
- 425 (13) Yost, S.R.; Lee, J.; Wilson, M.W.B.; Wu T.; McMahan, D.P.; Parkhurst, R.R.;
426 Thompson, N.J.; Congreve, D.N.; Rao, A.; Johnson, K.; Sfier, M.Y.; Bawendi, M.G.;
427 Swager, T.M.; Friend, R.H.; Baldo, M.A.; Van Voorhis, T.; A transferable model for
428 singlet-fission kinetics. *Nat. Chem.* **6**, 492-497 (2014)
- 429 (14) Odom, S. A.; Parkin, S. R.; Anthony, J. E. Tetracene derivatives as potential
430 red emitters for organic LEDs. *Org. lett.* **5**, 4245–8 (2003)
- 431 (15) Stern, H. L.; Musser, A. J.; Gelinas, S.; Parkinson, P.; Herz, L. M.; Bruzek,
432 M. J.; Anthony, J.; Friend, R. H.; Walker, B. J. Identification of a triplet pair
433 intermediate in singlet exciton fission in solution. *PNAS* **112**, 7656-7661 (2015)
- 434 (16) Liebel, M.; Kukura, P.; Broad-band impulsive vibrational spectroscopy of
435 excited electronic states in the time domain. *J. Phys. Chem. Letts.* **4**(8) 1358-1364
436 (2013)
- 437 (17) Rafiq, S. ; Scholes, G.D. ; Slow Intramolecular Vibrational Relaxation Leads
438 to Long-Lived Excited-State Wavepackets. *J. Phys. Chem. A.* **120**, 6792–6799
439 (2016).
- 440 (18) Berkelbach, T.C.; Hybertson, .S.; Reichman, .R.; Microscopic theory of
441 singlet exciton fission. I. General formulation. *J. Chem. Phys.* **138**, 114102 (2013)
- 442 (19) Fuemmeler, E.G.; Sanders, S. N.; Pun, A.P.; Kumarasamy, E.; Zeng, T.;
443 Miyata, K.; Steigerwald, M.L.; Zhu, X.Y.; Sfier, M.Y.; Campos, L.M.; Ananth, N.; A
444 direct mechanism of ultrafast intramolecular singlet fission in pentacene dimers. *ACS*
445 *Central Science*, **2**, 316-324 (2016)
- 446 (20) Bakulin, A. A.; Morgan, S. E.; Kehoe, T. B.; Wilson, M. B.; Chin, A.;
447 Zigmantas, D.; Egorova, D.; Rao, A, Real-time observation of multiexcitonic states in
448 ultrafast singlet fission using coherent 2D electronic spectroscopy. *Nat. Chem.* **8**, 16-
449 23 (2016)
- 450 (21) Musser, A. J.; Liebel, M. Schnedermann, C.; Wende, T.; Kehoe, T.B.; Rao,
451 A.; Kukura, P.; Evidence for conical intersection dynamics mediating ultrafast singlet
452 exciton fission. *Nat. Phys.* **11**, 352-357 (2014)
- 453 (22) Monahan, N. R.; Sun, D.; Tamura, H.; Williams, K. W.; Xu, B.; Zhong, Y.;
454 Kumar, B.; Nuckolls, C.; Harutyunyun, A. R.; Chen, G.; Dai, H-L.; Beljonne, D.;
455 Rao, Y.; Zhu, X-Y. Dynamics of the triplet-pair state reveals the likely coexistence of
456 coherent and incoherent singlet fission in crystalline hexacene. *Nature Chem*,
457 doi:10.1038/nchem.2665 (2016)
- 458 (23) Liebel, M.; Schnedermann, C.; Kukura,P.; Vibrationally coherent crossing
459 and coupling of electronic states during internal conversion in β -carotene. *Phys. Rev.*
460 *Letts.* **112**, 198302 (2014)

- 461 (24) Tiwari, V.; Peters, W. K.; Jonas, D. M.; Electronic resonance with
462 anticorrelated pigment vibrations drives photosynthetic energy transfer outside the
463 adiabatic framework. *PNAS*, **110**, 1203-1208 (2013)
- 464 (25) Casanova, D.; Electronic structure study of singlet fission in tetracene
465 derivatives. *J. Chem. Theory Comput.* **10**, 324-334 (2014)
- 466 (26) Chan, WL.; Ligges, M.; Zhu XY.; The energy barrier in singlet fission can be
467 overcome through coherent coupling and entropic gain. *Nat. Chem.* **4**, 840-5 (2012)
- 468 (27) Arias, D.H.; Ryerson, J.L.; Cook, J.D.; Damauer, NH.; Johnson, J.C.
469 Polymorphism influences singlet fission rates in tetracene thin films. *Chemical*
470 *Science*, **7**, 1185 (2016)
- 471 (28) Miyata, K.; Kurashige, Y.; Watanabe, K.; Sugimoto, T.; Takashi, S.; Tanaka,
472 S.; Takeya, J.; Yanai, T.; Matsumoto Y.; *Nat. Chem.* doi:10.1038/nchem.2784 (2017)
- 473 (29) Chang, T-C.; Dlott, D.D.; Picosecond vibrational cooling in mixed molecular
474 crystals studied with a new coherent raman scattering technique. *Chem. Phys. Lett.*
475 **147**, 18-24 (1988)
- 476 (30) Gelinias, S.; Par, O.; Brosseau, C. N.; Albert-Seifried, S.; Mcneill, C. R.;
477 Kirov, K. R.; Howard, I. A.; Leonelli, R.; Friend, R. H.; Silva, C.; Centreville, S.
478 Binding energy of charge-transfer excitons localized at polymeric semiconductor
479 heterojunctions. *J. Phys. Chem.* **115**, 7114–7119 (2011)
- 480 (31) Pensack, R. D.; Ostroumov, E. E.; Tilley, A. J.; Mazza, S.; Grieco, C.;
481 Thorley, K. J.; Asbury, J. B.; Seferos, D. S.; Anthony, J. E.; Scholes, G. D.
482 Observation of two triplet-pair intermediates in singlet exciton fission. *J. Phys. Chem.*
483 *Lett.* **7**, 2370-2375 (2016)
- 484 (32) Yost, S.R.; Hontz, E.; Yeganeh, S.; Van Voorhis, T.; Observation of Two
485 Triplet-Pair Intermediates in Singlet Exciton Fission. *J. Phys. Chem. C*, **116**, 17369-
486 17377 (2012)
- 487 (33) Burdett, J.J.; Bardeen, C. J.; Quantum beats in crystalline tetracene delayed
488 fluorescence due to triplet pair coherences produced by direct singlet fission. *JACS*
489 **134**, 8597-607 (2012)
- 490 (34) Keong Yong, C.; Musser, A.J.; Bayliss, S.L.; Lukman, S.; Tamura, H.;
491 Bubnova, O.; Hallani, R.K.; Meneau, A.; Resel, R.; Maruyama, M.; Hotta, S.; Herz,
492 L.M.; Beljonne, D.; Anthony, J. E.; Clark, J.; Siringhaus, H.; The entangled triplet
493 pair state in acene and heteroacene materials. *Nat. Comms*, **8**, DOI:
494 10.1038/ncomms15953 (2017)
- 495 (35) Thorsmølle, V.; Averitt, R.; Demsar, J.; Smith, D.; Tretiak, S.; Martin, R.;
496 Chi, X.; Crone, B.; Ramirez, a.; Taylor, a. Morphology Effectively Controls Singlet-
497 Triplet Exciton Relaxation and Charge Transport in Organic Semiconductors. *Phys.*
498 *Rev. Lett.* **102**, 017401 (2009)
- 499 (36) Kolomeisky, A.B.; Feng, X.; Krylov, A. I.; A simple kinetic model for singlet
500 fission: A role of electronic and entropic contributions to macroscopic rates. *J. Phys.*
501 *Chem.* **118**, 5188-5195 (2014)
- 502 (37) Odom, S.; Parkin, S. R.; Anthony, J. E. *Organic letters*, 2003 , 5 , 4245-8.
- 503 (38) Chen K, Gallaher JK, Barker AJ, Hodgkiss JM, *J. Phys. Chem. Lett*, 2014,
504 5(10), 1732-1737.
- 505 (39) Rao, A.; Wilson, M.; Hodgkiss, J. M.; Sei, Basser, H.; Friend, R.H.; *Journal*
506 *of the American Chemical Society* 2010, 132, 12698-12703.

509 Acknowledgments

510 The authors thank the Winton Programme for the Physics of Sustainability and the
511 EPSRC for funding. RHF thanks the Miller Institute for Basic Research and the
512 Heising-Simons Foundation at UC Berkeley for support. The authors thank Dr. T.
513 Arnold (Diamond Light Source), Dr. J. Novak, D. Harkin and J. Rozboril for support
514 during the beamtime at beamline I07 and the Diamond Light Source for financial
515 support. The computational work was supported by the Scientific Discovery through
516 Advanced Computing (SciDAC) program funded by the U.S. Department of Energy,
517 Office of Science, Advanced Scientific Computing Research, and Basic Energy
518 Sciences.

519

520 **Author Contributions**

521 H.L.S and A.C carried out the experiments, interpreted the data and wrote the
522 manuscript. SRY and MHG ran calculations, interpreted the data and wrote the
523 manuscript. NCG and SB interpreted the data. KB, AC, KC and JH performed
524 experiments. KT and JA designed and synthesized the materials. AR, AJM and RHF
525 interpreted the data and wrote the manuscript. All authors discussed the results and
526 commented on the manuscript.

527

528 **Additional information**

529 Supplementary information is available in the online version of the paper. Reprints
530 and permissions information is available online at www.nature.com/reprints.

531 Correspondence and requests for materials should be addressed to A.R. or R.H.F.

532

533 **Competing financial interests**

534 The authors declare no competing financial interests.

535

536

537 **Figure captions:**

538

539 Figure 1: TIPS-tetracene energies and structure (a) Energy level diagram of TIPS-
540 tetracene. The S_1 energy is determined from the UV-vis spectra (c) whilst the T_1
541 energy is estimated from phosphorescence measurements¹⁵. (b) TIPS-tetracene
542 chemical structure and one unit cell of the TIPS-tetracene crystal structure. (c)
543 Normalized UV-vis absorption and steady-state emission of the disordered film
544 (purple) and dilute solution (3 mg/ml in chloroform) (grey) and the excitation and
545 emission spectra of the polycrystalline film (green).

546

547 Figure 2. Ultrafast TT formation. (a) and (b) Ultrafast transient absorption
548 measurements of disordered and polycrystalline TIPS-tetracene films from 50 fs – 90
549 ps. We note the polycrystalline film measurement is affected by pump scatter in the
550 SE spectral region. (c) Transient absorption spectra of S_1 , from a measurement of
551 solution, and TT, from a measurement of a polycrystalline film at a time delay of 100
552 ps. (c) and (d) Normalised kinetics (normalised at 2 ps) obtained from the
553 measurements in (a) and (b) respectively. (c) For the disordered film, the kinetic
554 representing the decay of the SE is taken at 570 nm. For the rise of the TT state we
555 plot the difference between the change in absorption at 860 nm (a TT absorption
556 peak) and 835 nm. The two kinetics are normalised at 0 fs and subtracted. At the
557 beginning of the measurement both regions contain S_1 absorption and the difference
558 in the kinetics represents the growth of TT. (d) For the polycrystalline film the loss of
559 SE intensity is represented at 580 nm where there is slightly decreased pump scatter.

560 The TT kinetic is the difference in absorption intensity between 860 nm and 835 nm,
561 as in the disordered film.

562

563 Figure 3: Vibrationally coherent TT formation. (a) Vibrational frequencies of TIPS-
564 tetracene obtained from the ultrafast transient absorption measurements, from 0-2 ps,
565 of solution (grey), disordered film (purple) and the polycrystalline film (green) and
566 the ground state resonance Raman spectrum (black). The highlighted regions indicate
567 a prominent S_1 frequency at 315 cm^{-1} (blue shading) and new modes that exist in the
568 films and not in either solution or ground state (GS) Raman at 760 cm^{-1} , 870 cm^{-1} and
569 1090 cm^{-1} (red shading). (b) The spectral slices of the 315 cm^{-1} and 760 cm^{-1} modes
570 and timeslices from the transient absorption measurements of the polycrystalline film,
571 taken at 50 fs and 90 ps. (c) Sliding-window Fourier transform plots of the 315 cm^{-1}
572 and 760 cm^{-1} modes in the polycrystalline film, obtained at 570 nm for the 315 cm^{-1}
573 mode and 850 nm for the 760 cm^{-1} mode. The sliding window Fourier transform was
574 performed by sliding a 1 ps time window from 0 fs to 2 ps. The x axis represents the
575 starting time for the sliding window.

576

577 Figure 4. Thermally-activated TT separation. (a,c,e) Transient absorption spectra from
578 1 ns to 3 μs of the (a) concentrated solution, (c) disordered film and (e)
579 polycrystalline film in the near-IR spectral region. For the concentrated solution and
580 disordered film we observe two decay regimes that can be spectrally deconvoluted
581 using a code based on a genetic algorithm (see SI for details) into two distinct spectra
582 corresponding to TT and $T_1 + T_1$. The TT spectrum contains additional absorption
583 intensity between the two peaks at 850 nm and 960 nm and the peaks are blue-shifted
584 by 5 meV. (b,d) The extracted room temperature kinetics for the TT and T_1 decay in

585 the (b) concentrated solution and (d) the disordered film. The photoluminescence
586 decay of the TT state at room temperature in the concentrated solution and at 10 K in
587 the disordered film are shown plotted against the TA decay (purple trace). (f) Raw
588 kinetics from the transient absorption measurement of the disordered and
589 polycrystalline films at 850 nm highlighting the different decay behaviour.

590

591 Figure 5: Thermally-activated TT emission. (a,d) Time-resolved emission scans
592 reveal two emissive states in both the (a) disordered film and (d) polycrystalline films
593 at 10 K. PL Count represents the photoluminescence intensity. The emission from 30-
594 100 ns is shown magnified for the crystalline film (inset (d)). Timeslices at 0.5 ns and
595 50 ns are shown above the colour plots. (b,e) Temperature-dependent kinetics taken at
596 540 nm and 600 nm for the (b) disordered and (e) polycrystalline films. We obtained
597 an activation energy in the red-shifted region of ~90 meV and ~50 meV respectively.
598 (c,f) Temperature-dependent steady-state emission for the (c) disordered and (f)
599 polycrystalline films. The spectra are normalised to the peak of the emission at 10 K.
600 At higher temperatures the spectra are plotted to show their intensity relative to the 10
601 K emission.

602

603 Figure 6: The role of the TT state in endothermic singlet exciton fission.

604 (Top) A schematic diagram of endothermic singlet exciton fission. The wavepacket
605 generated at the Franck Condon (FC) position of the S_1 potential energy surface is
606 passed to the TT state during ultrafast formation of TT. Thermally-activated TT
607 separation occurs over tens of nanoseconds. (Bottom) The kinetics of the S_1 , TT and
608 $T_1 + T_1$ species in the disordered film from 10 fs to 100 μ s, obtained from the TA
609 measurements using a genetic algorithm for spectral deconvolution.

610

611

612